



Intermolecular Structural Correlations in Model Globular and Unconcatenated Ring Polymer Liquids

Journal:	<i>Soft Matter</i>
Manuscript ID	SM-ART-08-2018-001722.R2
Article Type:	Paper
Date Submitted by the Author:	29-Oct-2018
Complete List of Authors:	Dell, Zachary; University of Massachusetts Amherst, Polymer Science and Engineering Schweizer, Kenneth; University of Illinois at Urbana-Champaign,

Soft Matter, submitted, August, 2018; revision submitted October 2018

**Intermolecular Structural Correlations in Model Globular and
Unconcatenated Ring Polymer Liquids**

Zachary E. Dell¹ and Kenneth S. Schweizer^{2-4*}

Department of Polymer Science and Engineering¹, University of Massachusetts, Amherst,
MA, 01003

Departments of Materials Science² Chemistry³, Chemical & Biomolecular Engineering⁴
and Frederick Seitz Materials Research Laboratory⁵, University of Illinois, Urbana, IL
61801 USA

[*kschweiz@illinois.edu](mailto:kschweiz@illinois.edu)

Abstract

We employ the field theoretic polymer integral equation theory to construct a segment-level theory for the thermodynamics and pair structure of dense liquids of interpenetrating ring polymers and a simple globule model. The latter is defined by a fractal mass distribution on all internal length scales with an exponent equal to the spatial dimension ($d_F=d_s=3$). In an isochoric ensemble the dimensionless compressibility and pressure is predicted to vary exponentially with macromolecular volume fraction. An inter-molecular correlation hole exists down to small length scales. This model appears to be useful for a recently studied experimental soft nanoparticle suspension, and also serves as a reference system for our analysis of ring liquids. Motivated by simulations, a two-fractal exponent ring model is adopted for the intra-molecular structure factor. At smaller lengths it describes chain-like macromolecules, while on larger scales it corresponds to a space-filling object in the sense that $d_F=d_s=3$. The crossover between these two regimes is of order the entanglement length of the linear chain analog. Based on a constant compressibility ensemble, the effective volume fraction grows at intermediate values of degree of polymerization (N), and crosses over to a very slow logarithmic growth at large N . A weaker intermolecular correlation hole is predicted. The number of nearest neighbor rings increases dramatically at small N , akin to linear chain melts, but then tends to saturate at large N , in accord with simulations. The tools developed may be relevant for other partially interpenetrating soft objects such as core-shell nanogels or microgels.

I. INTRODUCTION

Macromolecular science and engineering is a vibrant field due to remarkable advances in synthesis, the rich array of physical phenomena polymers display, and their many useful properties and applications [1–6]. Particularly fascinating and unique are the consequences of topological interactions on dynamical and mechanical behavior, due microscopically to the combined constraints of polymer connectivity and dynamic uncrossability [2–5,7,8]. While there have been many studies of linear chains and controllably branched (e.g., stars, combs) polymer liquids [4,5], other macromolecular architectures with compact features have only recently begun to be studied. Of specific interest here are dense liquids composed of a simple globule model and unconcatenated (no knots) ring polymers [5,8–17].

Both cyclic ring polymers and compact globule-like polymeric objects are relevant in diverse areas of physics, chemistry, materials science, and also cellular biology. So-called "single chain nanoparticles" with a globule-like character have been created from synthetic polymers and studied in solution and nanocomposites [18–22]. More generally, the intramolecular collapse of polymer chains to form nanogel or microgel particles is a rich field in soft materials science including the area of drug delivery [23–25]. In biology, proteins, DNA, and RNA can take on globally compact or collapsed conformations with diverse internal microstructures [26–28]. Biopolymers, such as DNA, can exist in the end-free circular form [29,30]. Driven largely by simulation [11,31–43], there has been much recent interest in the polymer physics of the structure and dynamics of unconcatenated ring polymer liquids, including their possible relevance to the problem of chromatin organization and viral nucleic acid packaging

[8,26,29,30,42,43]. Even though the DNA in a chromatin is a linear chain, its exceptionally long length may effectively quench large scale equilibration processes (e.g., reptation) [8,42]. One possible consequence is the emergence, for large enough rings, of effectively static (on cellular time scales) topological effects leading to chromatin forming globally compact structures or "territories", albeit with strongly fluctuating interfaces that allow significant interpenetration [8].

As relevant background for our present work, we summarize some key recent experimental [16, 44–46], theoretical [47], and simulation [11,32–43] findings for unconcatenated ring polymer liquids. In both melts and semidilute solutions, for a sufficiently large degree of polymerization (N) the rings acquire a drastically different conformational structure compared to their linear chain analogs [8,45–47]. Specifically, they are akin to collapsed globules on global length scales in the sense that the radius of gyration scales with degree of polymerization as $R_g \sim N^{1/3}$ but also form *partially*-segregated "territories". A caveat is that not all published simulations have definitively established that the R_g versus N scaling exponent in dense melts and solutions is $1/3$ [8]. On more local length scales, the internal microstructure of rings in dense liquids is found to be more chain-like in an ensemble-averaged sense and hence described by a smaller effective fractal dimension than $d_F = 3$. The length scale characterizing this crossover from global to local behavior appears to be close to the intrinsic N -independent entanglement length of the linear chain analog [32–34,47]. This crossover is expected to have major structural and dynamic consequences. For example, simulations find the number of rings interpenetrating a tagged ring approaches a finite (model-dependent) limit of order 5–20 at high enough N [32–34], in contrast to ideal chains ($d_F = 2$) where

there is unbounded growth and the number of interpenetrating chains scales as $\sim N^{1/2}$ [2,3,48]. Visually, simulations find individual rings have a very rough fluctuating "surface" and "protrusions" which allows copious interpenetration (or "threading") with other rings in a dense liquid [8,32-34]. The limited neutron scattering studies of ring structure appear to be consistent with these simulation findings [45,46].

The goal of this article is to construct minimalist coarse-grained polymer models, and use them in conjunction with liquid state polymeric integral equation theory *at the segment level*, to predict the equilibrium collective and intermolecular packing structure of dense fluids of globules and unconcatenated ring polymers. Our working hypothesis is that an ensemble-averaged description of *single* macromolecule structure at the *pair* correlation level is adequate to make useful predictions for the *intermolecular* pair correlations on the segmental level. This is the established philosophy of polymer liquid state theory [49,50] which has proven to be useful for interpenetrating chain liquids. To the best of our knowledge, our present work is the first theoretical attempt to predict the intermolecular and collective pair structure at the segmental level of dense liquids of globules or rings. However, we recognize that rings are unusual objects where so-called "threading" and perhaps other aspects may not be fully captured at the pair correlation level. But the predictions we make can be tested against future simulations and/or experiments, and some of this is carried out here for the globule and ring liquids with encouraging results demonstrated.

We employ the simplest field-theoretic "thread limit" version of the polymer reference interaction site model (PRISM) integral equation approach, where hard core intermolecular segment–segment repulsions correspond to a point-like excluded volume

constraint [49,50]. As input to the theory, we adopt two simple models for the intramolecular structure factor (Figure 1): (i) a single fractal model of a globule (Fig. 1a), and (ii) a partially interpenetrating, two fractal ring model (Fig. 1b).

We are not claiming that model (i) is an accurate description of any specific soft matter system. Rather, our two-fold motivation for studying it is as follows. First, it seems to us to be the simplest model of a collapsed globule-like object ($d_F = 3$ on all internal length scales) with no sharp (Porod-like) interface. Moreover, as we demonstrate in Section II.C., this model appears to be useful for understanding unusual thermodynamic properties of dense suspensions of phytoglycogen soft particles with thin or non-existent coronas. Second, the model serves as an instructive, albeit oversimplified [32-34], reference system for comparison with our results for ring liquids. Model (ii) is constructed based on simulation information [32-34] for the *intra*-ring pair correlations in the condensed state. In addition to the inter-molecular segment-segment pair correlation function and collective static structure factor— $g(r)$ and $S(k)$, respectively—we make predictions for thermodynamic properties (dimensionless compressibility, pressure) and the statistically defined number of nearest neighbors in a liquid.

For the simple globule model, we emphasize that we do *not* follow the usual approach to modeling soft fluctuating particles which performs an a priori averaging over of internal polymeric (segmental) degrees of freedom. Such approaches typically first determine a two-particle effective interaction, a potential of mean force (PMF) $W(r)$, between the centers-of-mass (CM) of a pair of *isolated* polymeric particles by ensemble averaging over or integrating out of all internal degrees of freedom [51,52]. This $W(r)$ is then used in soft sphere simulations or theory based on the assumption of pair

decomposability. The latter approximation generally fails at high enough concentrations where soft particles overlap and many-body correlations emerge. Moreover, it cannot address the intermolecular correlations at the segmental or elementary "site" level. Since we do not integrate out segment scale density fluctuations, many body effects at the CM level are approximately retained through all orders, and inter-segmental packing correlations are predicted. Because we analyze the simple globule model at the segmental level, it can experience some interpenetration on a small scale. Any possible "faceting" of globules at ultra-high volume fractions is not addressed at the level of description we employ.

There are multiple advantages of working at the segment level beyond what is stated above. It allows a fundamental connection to be made between structure and thermodynamics, and even dynamics [53,54], since the real interactions and forces between soft particles are on the local segmental scale. Moreover, such an approach smoothly goes back to linear chain liquids within the same liquid state theory framework. This common description of compact soft particles and polymer coils allows us to compare their behavior in a direct manner. The present work also sets the stage for developing force and segment level theories for the slow dynamics of fluctuating soft particles in dense liquids. A disadvantage is structure at the CM level is not directly obtained. However, it can be determined based on well known approximate connections between the site and CM levels of description [51,52]. More generally, we believe the methods developed in this article are relevant to other liquids composed of soft fluctuating particles of diverse internal microstructures.

The remainder of the paper is structured as follows. Section II constructs the single polymer models studied and for context briefly reviews the relevant aspects of thread PRISM theory for chain polymer liquids. Sections III and IV present results for thermodynamic properties and inter-molecular structure of dense liquids of model globules and rings, respectively. The paper concludes in Section V with a discussion.

II. THEORY AND MODEL

We consider a liquid of n unconcatenated polymers each composed of N connected statistical segments (interaction sites) contained in a volume V . The total segment density is $\rho_s = N\rho = nN/V$, where ρ is the polymer molecule density. The elementary sites or segments are considered to be statistically equivalent with regards to the intermolecular ensemble-averaged *site–site* pair correlation function, $g(r)$. This simplification ignores small chain end effects. However, for collapsed globules and rings, chain ends effects are either not important or not present, although there are still topological effects [8–10].

A. Thread PRISM Theory

Thread PRISM theory [49] is the Edwards-like “field-theoretic”, largely analytic, limit of polymer integral equation theory, in which excluded volume interactions between sites or segments are reduced to a point-like non-overlap constraint (segment hard core diameter $d \rightarrow 0^+$). Consistent with this coarse graining of chemical features on the local scale, the chain consists of N connected segments of size σ with a radius-of-gyration $R_g^2 \propto \sigma^2 N^{1/d_F}$, where d_F is the polymer mass fractal dimension in the condensed phase [56–58]. For intermolecular pair correlations within the equivalent site framework, one starts with the generalized Ornstein–Zernike (Chandler–Andersen or PRISM) integral

equation theory for $g(r) = h(r) + 1$ of the homopolymer liquid, which in Fourier space is [49,55]:

$$h(k) = \omega(k)C(k)[\omega(k) + \rho_s h(k)] = \omega(k)C(k)S(k). \quad (1)$$

Here, $h(r)$ is the non-random part of the segment–segment pair distribution function, and $C(k)$ is segment-segment direct correlation function (effective intermolecular repulsion) in Fourier space. The intramolecular and collective structure factors are given by $\omega(k)$ and $S(k)$, respectively, where $\omega(k=0) = N$ and the second equality in Eq. (1) defines a functional relationship between $S(k)$, $\omega(k)$, and $h(k)$. Given knowledge of the ensemble-averaged single polymer structure factor, $\omega(k)$, and $C(k)$, PRISM theory predicts the intermolecular and collective pair structure encoded in the site-site level $g(r)$ and $S(k)$ and thermodynamic properties.

Closure of the PRISM equation requires (i) a relationship between $C(r)$, the segment-level pair potential $U(r)$, and $g(r)$, and (ii) a model for $\omega(k)$. For (i) we employ the standard site–site Percus–Yevick (PY) closure [49,55] which for hard core repulsions in the thread limit corresponds to:

$$C(r) = C_0 \delta(\vec{r}), \quad (2)$$

where $C(k=0) = C_0$. Combining Eqs. (1) and (2) gives the collective structure factor:

$$S(k) = \frac{S_0}{1 + S_0(\omega^{-1}(k) - N^{-1})} \quad (3)$$

where $S_0 = (N^{-1} - \rho_s C_0)^{-1}$.

Here, $S_0 = S(k=0)$ characterizes the dimensionless amplitude of long wavelength density fluctuations:

$$\frac{S_0}{N} = \rho k_B T \kappa_T = \left(\frac{\partial \beta P}{\partial \rho} \right)^{-1}, \quad (4)$$

where $k_B T = \beta^{-1}$ is the thermal energy and κ_T is the isothermal compressibility. The second equality is an exact relation between S_0 and the fluid pressure, P .

The exact inter-site non-overlap condition is then enforced, $g(r=0) = 0$. To implement this, we employ the Fourier transform:

$$h(r) = \int \frac{d\vec{k}}{2\pi^3} e^{i\vec{k} \cdot \vec{r}} h(k). \quad (5)$$

Combining Eqs. (1)–(5), and non-dimensionalizing the wave vector by the polymer radius of gyration, $q = kR_g$, we obtain:

$$h(\tilde{r}) = \frac{2}{3\pi\phi} \left(\frac{S_0}{N} - 1 \right) \int_0^\infty dq q^2 \frac{\omega(q)/N}{1 + (S_0/N)(N\omega^{-1}(q) - 1)} \frac{\sin q\tilde{r}}{q\tilde{r}}, \quad (6)$$

where a ‘‘macromolecular’’ volume fraction and dimensionless inter-site separation are defined as $\phi = 4\pi R_g^3 \rho / 3$ and $\tilde{r} = r/R_g$, respectively. The explicit core exclusion condition then becomes:

$$-h(r=0) = 1 = \frac{2}{3\pi\phi} \left(1 - \frac{S_0}{N} \right) \int_0^\infty dq q^2 \frac{\omega(q)/N}{1 + (S_0/N)(N\omega^{-1}(q) - 1)}. \quad (7)$$

For a given $\omega(k)$, Eq. (7) provides a nonlinear algebraic relationship between ϕ , S_0 (or C_0) and N , which mathematically closes thread PRISM theory.

Given $g(r)$, the number of neighboring segments *on other polymers* within a radius r^* of a segment on a tagged polymer, defined as n_s , is:

$$n_s(r^*) = 4\pi\rho_s \int_0^{r^*} dr r^2 g(r). \quad (8)$$

The number of neighboring polymer molecules surrounding a tagged polymer follows as

$n_p = n_s/N$. Non-dimensionalizing the integral in Eq. (8) via $\tilde{R} = r^*/R_g$ then yields n_p as a function of the averaging radius:

$$n_p(\tilde{R}) = 3\phi \int_0^{\tilde{R}} dx x^2 g(x). \quad (9)$$

Generically, for all connected macromolecules $g(r)$ cannot attain its random value of unity until sites are separated beyond R_g . This fact implies for $r^* \sim R_g$ that:

$$n_p(\tilde{R} \sim 1) \approx \frac{\rho_s R_g^3}{N} = \rho R_g^3. \quad (10)$$

For a large space-filling object, this quantity is of order unity (N -independent) in a dense liquid. For a fractal macromolecule (d_F less than the space dimension, d_S), it grows without bound with N . To proceed further, a specific form of $\omega(k)$ is needed. We first recall relevant prior results of thread PRISM theory for ideal random coil liquids.

B. Linear Chains

Thread PRISM theory models flexible chains as Gaussian threads with an intramolecular structure factor that properly captures the power law scaling behavior of an ideal random walk on intermediate length scales (or wave vectors):

$$\omega(k) = \frac{1}{N^{-1} + (k\sigma)^2/12} = \frac{N}{1 + (kR_g)^2/2}. \quad (11)$$

Solving the PRISM equation yields the *inter*-chain segment–segment pair correlation function:

$$g(r) = 1 + \frac{3}{\pi\rho_s\sigma^2} \frac{e^{-r/\xi_p} - e^{-\sqrt{2}r/R_g}}{r}, \quad (12)$$

where the density correlation or physical mesh length ξ_p is:

$$\xi_p^{-1} = \frac{\pi}{3} \rho_s \sigma^2 + \frac{\sqrt{2}}{R_g} \approx \rho_s \sigma^2 = p^{-1}. \quad (13)$$

Here the approximate equality holds in the limit $\rho \gg \rho^*$, where ρ^* denotes the dilute-to-semi-dilute crossover. For densities well above ρ^* , the mesh length essentially equals the so-called invariant (to coarse graining) "packing length", p [48,49]. The first term on the right-hand side of Eq. (12) is the mean field (random structure) result, while the second term describes local screening of segmental density fluctuations, and the third (negative) term is the universal long range deGennes correlation hole contribution [3,49]. Substituting Eq. (12) in Eq. (9) predicts for ideal coil liquids at concentrations well above ρ^* the known scaling $n_p(r^* \sim R_g) \propto \sqrt{N}$.

Under Θ solvent (ideal conformation) or dense melt conditions, σ is independent of polymer concentration, and $\xi_p \propto \phi_s^{-1}$, where $\phi_s = \rho_s \pi \sigma^3 / 6$ is the segment volume fraction. In athermal good solvents $\sigma \propto \phi_s^{-1/8}$, and thus $\xi_p \propto \phi_s^{-3/4}$ is predicted. These results agree with the blob scaling laws of deGennes (using the mean field Flory exponents) [2,3], as do the thread PRISM theory predictions [49] for the osmotic pressure in Θ and good semi-dilute solutions. The collective static structure factor is a Lorentzian, $S(k) = S_0(1 + k^2 \xi_p^2)^{-1}$, where the dimensionless compressibility is given by:

$$S_0 = 12 \left(\frac{\xi_p}{\sigma} \right)^2. \quad (14)$$

C. Simple Globule Model

Our minimalist one fractal exponent model of globules is *defined* via the following intra-molecular structure factor [56–58]:

$$\omega(k) = \frac{N}{1 + A(kR_g)^{d_F}}, \quad (15)$$

where the constant A depends only on fractal and spatial dimensions. For the 3D globules of interest here, $d_F = d_S = 3$, and the radius of gyration is:

$$R_g^{d_F} = C N \sigma^{d_F}. \quad (16)$$

where C is a constant. This model not only obeys the global scaling law $R_g \sim N^{1/3}$, but also adopts a self-similar scaling of the internal pair density correlations with $d_F = d_S = 3$. While the constant A can be chosen to model various specific globular objects, here for both concreteness, and to allow us to directly compare the globule and ring liquids results, we choose A using the intra-molecular structure factor from a recent ring polymer liquid simulation [33] by fitting Eq. (15) to the data in the lower wavevector regime. Figure 2 shows the simulation results [33] (different data point types represent different ring sizes) and the black curve shows the fit using Eq. (15). In the low wave vector regime ($kR_g \lesssim 5$), the results for all ring sizes collapse and $A = 0.286$. The simple globule model is thus *defined* by employing this low wave vector form on all length scales per Eq. (15). At larger wave vectors, the simulation data of Fig. 2 deviates from this form because locally rings become chain-like. At even higher wavevectors non-universal local features are present (see Section II.D).

Based on Eq. (15), Eq. (7) can be analytically evaluated for $d_F = 3$, yielding:

$$1 = \frac{2}{9\pi A \phi} \ln \left(\frac{N}{S_0} \right) \Rightarrow \frac{S_0}{N} = e^{-9\pi A \phi / 2}. \quad (17)$$

Note the interesting, and seemingly novel, exponential dependence of the dimensionless compressibility on macromolecular volume fraction. The pressure follows from Eq. (4), which when combined with Eq. (17), and performing the necessary integral, yields:

$$\beta P = \int_0^\rho d\rho' \frac{N}{S_0(\rho')} \quad (18)$$

$$= \rho \left(\frac{e^{9\pi A\phi/2} - 1}{9\pi A\phi/2} \right) = \frac{1}{6R_g^3 A\pi^2} (e^{9\pi A\phi/2} - 1) \quad (19)$$

Thus, at high effective volume fractions the pressure also grows exponentially.

We note a very recent and interesting experimental study of dense suspensions of phytoglycogen soft particles (~ 30 nm diameter) which are highly branched objects with an internal dendritic structure [59]. Over the high effective volume fraction range of ~ 0.75 – 1.8 , the osmotic pressure was observed to grow strongly from ~ 5 kPa to 1 MPa, and to a very good approximation increases in an exponential manner as $\sim e^{5\phi}$. At an effective volume fraction of unity, it is ~ 15 kPa. To the best of our knowledge, there is no theoretical understanding of these observations. We now compare Eq. (19) with these experimental findings.

Using a constant diameter of 30 nm, Eq. (19) predicts a pressure of ~ 5 kPa for a volume fraction of unity, and over the experimental range an exponential growth of pressure of roughly $\sim e^{4\phi}$. No doubt our simple globule model is oversimplified compared to the precise (unknown) internal statistical structure of phytoglycan nanoparticles, but these very sensible predictions of Eq. (19) encourage a deeper study of this system using our theoretical approach. This will be possible, for example, if neutron scattering measurements are performed to determine the ensemble-averaged single particle structure factor. Now, at volume fractions beyond 2, the experimental osmotic pressure appears to grow very weakly and tends to saturate at ~ 2 MPa [59]. Such behavior is not captured by Eq. (19), which may indicate a "soft jamming" crossover and/or volume-

fraction-dependent nanoparticle compression at ultra-high loadings, physical effects not included in our present simple model.

Since the simple globule model is qualitatively space filling on *all* length scales, there is no intrinsic N -dependence of the thermodynamic properties if the colloid-like macromolecular volume fraction $\phi = (4\pi/3)\rho R_g^3$ is adopted. Finally, Eq. (17) is generic for globules in any space dimension ($d_F = d_S = d$); we find $1 = C_d \phi_d^{-1} \log(N/S_0)$, where C_d depends on d_S and $\phi_d \sim \rho R_g^d$ is the generalized d -dimensional volume fraction.

D. Interpenetrating Ring Model

To capture the computer simulated single ring structure factor [33] in the condensed state (Fig. 2), we adopt an analytic and minimalist two-fractal description with an intrinsic, N -independent, crossover length scale λ :

$$\omega(k) = \begin{cases} \frac{N}{1 + A(kR_g)^3} & k < \lambda^{-1} \\ \frac{N}{k^2(\lambda^2 + AR_g^3/\lambda)} & k \geq \lambda^{-1} \end{cases} . \quad (20)$$

Since there are now two length scales, N enters explicitly. For length scales larger than λ , the conformational structure is identical to our simple globule model. Recall this was one of the motivations for studying the latter model. However, on more local (but still large mesoscopic) length scales the ring behaves in an ensemble-averaged sense as an ideal random walk where $\omega(k) \sim k^{-2}$. The prefactor for $\omega(k \geq \lambda^{-1})$ is chosen to satisfy continuity of ω at the crossover wavevector $k = \lambda^{-1}$ and faithfully reproduce the simulation results [33].

To determine A and λ in Eq. (20), the simulation results for $\omega(k)$ are fit in the following manner. The constant A is determined from the simple globule model small

wavevector fit of $\omega(k)$ as discussed in the previous section, yielding $A = 0.286$. Based on this fit, the crossover length for each simulation data set can be approximately deduced as when the data falls off the $\sim k^{-3}$ scaling behavior in Figure 2. As physically expected, we find that this crossover roughly scales as $\lambda/R_g = \lambda_0/N^{1/3}$ where $\lambda_0 = 2.5$. This implies the crossover length is *intrinsic*, $\lambda \sim N^0$, and mesoscopic in the sense that $\sigma \ll \lambda < R_g$ for large N . Recent simulations [11,32–43] and theoretical studies [8,47] suggest the crossover length is set by intra-ring entanglements and is roughly the corresponding chain liquid entanglement length $\lambda \sim d_T = \sqrt{N_e} \sigma$, where N_e is the number of statistical segments between entanglements. The latter is typically cited as ~ 28 in the standard bead-spring Kremer–Grest model of dense melts, but is larger based on primitive path analysis [60] or in semi-dilute solutions [33]. We emphasize that for the sake of our work, understanding the specific physical cause of the crossover is *not* necessary. Rather, the important point is the two-fractal nature of the macromolecular structure with two length scales. In any case, the latter has a dramatic influence on the equilibrium properties of ring polymers and provides the mechanism for ring interpenetration in the condensed phase.

The dashed curves in Figure 2 show the fits of Eq. (20) to the simulation data, and one sees very good agreement in the mesoscopic regime. Note that, as expected, at very large k there are deviations due to local chemical structure effects, which are coarse grained over in the thread model. This regime does not affect our key conclusions.

Inserting Eq. (20) into the intermolecular excluded volume condition of Eq. (7), and analytically evaluating the integral, yields:

$$1 = \frac{2}{9\pi A \phi} \log \left[\frac{1 + AN/\lambda_0^3}{1 + S_0 A/\lambda_0^3} \right] + \frac{2}{3\pi \phi} \frac{(N/S_0 - 1)^{1/2}}{(\lambda^2 + A/\lambda)^{3/2}} \times \left[\frac{\pi}{2} - \arctan \left(\sqrt{\frac{(1 + A/\lambda^3)}{N/S_0 - 1}} \right) \right]. \quad (21)$$

Eq. (21) relates S_0 (or C_0), ϕ , λ_0 , and N for a liquid of interpenetrating rings and closes the thread PRISM theory. In the remaining sections we present the results of numerically solving the thread PRISM equations (Eqs. (3), (6), and (9)) for the two models of interest. All our results for ring polymer liquids are expected to be applicable only for concentrations high enough that Eq. (20) is valid.

III. STRUCTURAL RESULTS FOR THE SIMPLE GLOBULE MODEL LIQUID

For the globule model we study, the appropriate measure of dimensionless density is the macromolecular volume fraction, ϕ . For a given volume fraction and chain length N , Eq. (17) determines S_0 . The exponential relation between dimensionless compressibility and volume fraction is very different from its linear chain analog ($d_F = 2, d_S = 3$), where for large N one has $S_0 = 12(\xi_p/\sigma)^2 \sim p^2/\sigma^2$. From Eqs. (3), (6), (15) and (17), since $S_0 \sim N$ and $\omega(k) \sim N$, the resulting inter-molecular structure for globules is independent of N .

Figures 3 and 4 show results for the inter-molecular pair structure at various volume fractions. The so-defined macromolecular volume fraction can exceed $\phi = 1$ as is commonly the case for soft colloid microgels. Moreover, as mentioned in the Introduction, the globule is modeled at the segmental level and intermolecular repulsion on that scale does not completely prohibit limited interpenetration on the macromolecular scale. Figure 3 (main) presents the site–site pair distribution function as a function of

separation for volume fractions varying from $\phi = 0.1$ to 5. The pair distribution function has a deep correlation hole. This feature is not directly due to a CM level repulsive PMF per standard models [3,61], but rather follows from our explicit accounting of chain connectivity and uncrossability at the segmental level. As inter-site separation increases, $g(r)$ grows nearly monotonically until it approaches unity at large separations. We note for the highest volume fraction there is a very small overshoot region where $g(r) > 1$. It does not arise from a nonzero excluded volume of segments nor a k -dependent $C(k)$ as it does in atomic, molecular, or hard colloid fluids since sites in the polymeric thread model have a hard-core diameter $d \rightarrow 0$. Rather, it is the combined consequence of connectivity and point-like uncrossability. The inset of Fig. 3 quantifies the excess or nonrandom component of the intermolecular site–site correlations including the surface area factor, $(r/R_g)^2 h(r)$. The strongly damped oscillations about zero indicate weak liquid-like packing correlations on a macromolecular length scale.

It is interesting to compare the $g(r)$ of the simple globule model with its linear chain analog at the same macromolecular volume fraction. From Eq. (12), the latter follows in the variables relevant to the globule as:

$$g(\tilde{r}) = 1 + \frac{2 e^{-\alpha\tilde{r}} - e^{-\sqrt{2}\tilde{r}}}{3\phi \tilde{r}} \quad (22)$$

$$\alpha \equiv \frac{R_g}{\xi_p} = \sqrt{2} + \frac{3}{2} \phi, \quad (23)$$

where $\tilde{r} = r/R_g$. Figure 3 shows a comparison for $\phi = 1$. The primary difference is that there is a much sharper increase in the chain liquid and a faster recovery to the random correlation value of $g(r) = 1$. This is accompanied by weaker excess correlations for the

linear chain (inset). The main reason for these trends is clear: linear chains can *fully* interpenetrate, while globules cannot, leading to a deeper correlation hole.

Figure 4 (main) shows the site-level collective density fluctuation structure factor normalized by N as a function of dimensionless wave vector. For the lowest volume fraction $\phi = 0.1$, $S(k)$ is very similar to $\omega(k)$, as expected. For small wave vectors, $S(k)$ is constant and equals the dimensionless compressibility, S_0 . It crosses over to the scaling behavior, $\sim (k\sigma)^{-3}$, at larger wave vectors, $kR_g \gg 1$. As volume fraction increases, the dimensionless compressibility decreases according to Eq. (17) and the crossover to the globule behavior occurs at larger wave vectors (smaller length scales). This is equivalent to a narrowing or filling in of the correlation hole at larger volume fraction, as seen in the $g(r)$ results in Fig.3.

As a measure of macromolecular coordination number, the number of neighboring globules (n_p) within a distance r^* of a tagged globule is calculated using Eq. (9) with $\tilde{R} \equiv r^*/R_g = 1.0, 1.5, 2.0$. The results are shown in the inset of Figure 4 as a function of macromolecular volume fraction. As volume fraction increases, the number of nearest neighbor globules rapidly increases in a nearly linear manner; the slope is sensitive to the chosen dimensionless distance of inter-molecular separation that defines a neighbor. However, for all volume fractions studied n_p is independent of N . This is different than for chains where the number of neighbors grows as \sqrt{N} .

IV. INTERPENETRATING RING RESULTS

A. Model Parameters

While for the simple globule model the macromolecular volume fraction is the appropriate measure of dimensionless density, for rings this is not true. Moreover, we

find (as expected) from Eq. (21) that employing a literal constant *macromolecular* volume fraction (ϕ) ensemble yields a dimensionless compressibility S_0 that rather strongly depends on ring degree of polymerization, N . Such a trend is not physically expected under dense liquid conditions, and it also disagrees with simulations [8, 33–35] which find that the ring melt equation-of-state (EOS) is essentially identical to that of linear chains, unaffected by geometric or topological effects. Moreover, for chain and ring liquids the EOS is nearly N -independent, which implies $S_0 \sim N^0$. This follows because of the fundamental connection between the pressure, temperature, and dimensionless compressibility at the segment level, which is $\beta P = \int_0^{\rho_s} d\rho'_s S_0^{-1}(\rho'_s)$. To leading order, this exact relation implies under isobaric and isothermal conditions that S_0 is essentially independent of N , as discussed previously for chain polymer melts [62]. Thus, we implement our ring liquid model in a "constant dimensionless compressibility ensemble" [62] defined as adopting a fixed, N -independent, value of S_0 . The precise magnitude of the latter can vary with local chemistry, polymer concentration, and degree of coarse graining. At a fixed S_0 , the corresponding effective volume fraction is then determined by solving Eq. (21). As discussed below, the latter becomes a relatively weak but nontrivial varying function of N to maintain the constant compressibility constraint.

In order to choose appropriate values of S_0 , we first consider a melt of linear thread chains described at the identical level of coarse graining with the same formulation of PRISM theory. To estimate S_0 requires values of the packing length and segment size. While for chain melts the packing length can vary over the range $p \approx 0.15\text{--}0.4$ nm [48] and is scale-invariant, the statistical segment size carries uncertainty since it is sensitive to the degree of local coarse graining. We employ several standard models to estimate σ :

the Kuhn length $\sigma_k \simeq C_\infty l_b$, the persistence length ($\approx 0.5 \sigma_k$), and the statistical length ($\sqrt{C_\infty} l_b$, $C_\infty \sim 4 - 10$) where l_b is the backbone chemical bond length (~ 0.15 nm) [2,48]. For ideal chains, it is known that $\omega(k) = 12(k\sigma)^{-2}$, where $\sigma = \sqrt{C_\infty} l_b$, in the intermediate scaling regime [2,3,49]. As an example, for polystyrene (PS) melts [48], $p \approx 0.4$ nm and $\sigma_k \approx 1.5$ nm, yielding $S_0 \approx 0.8$. If one uses the persistence length then $S_0 \approx 2$, and if one uses the statistical length ($\sigma_s \approx 0.45$ nm) then $S_0 \approx 9$. Thus, the melt dimensionless compressibility can vary by a factor of ~ 10 even for fixed chemistry. To cover these possibilities (chemical variations, as well as concentrated solutions versus melts) we adopt values of S_0 between 0.3 and 15 in our numerical work.

B. Results

Given S_0 and N as input, Eq. (21) determines the effective macromolecular volume fraction of the ring liquid. The main frame of Figure 5 shows in a linear–log representation the effective volume fraction ϕ_{eff} as a function of N for $S_0 = 0.3$ to 15; the inset shows the corresponding log–log plot. In the linear–log representation all curves are of a sigmoidal form. Moreover, for small N the effective volume fraction is always very low. As N increases from ~ 10 to 500, there is a dramatic increase in the effective volume fraction. Finally, at large N the effective volume fraction displays a quasi-plateau although it continues to grow slowly as $\phi_{eff} \sim \log N$. In this regime ϕ_{eff} ranges roughly from ~ 18 for $S_0 = 0.3$ down to ~ 5 for $S_0 = 15$.

A second way to analyze the effective volume fraction is to calculate N/ϕ_{eff} as a function of N . For all dimensionless compressibilities studied, we find (not shown) that at small N this quantity is roughly constant, at most varying by a factor of 2. At large N , there is a crossover to linear behavior where $N/\phi_{eff} \sim N$ due to the roughly constant

plateau of ϕ_{eff} at large N . This reflects the crossover behavior of the two-length scale ring model. For intermediate N , the dramatic increase of the effective volume fraction is akin to that of interpenetrating chain polymers. However, at large N the effective volume fraction is limited by the space-filling nature of rings on large length scales.

For chosen values of S_0 and N , the effective volume fraction, and thus the ring liquid intermolecular structure, can be calculated using Eqs. (3), (6), (9), and (20). Figure 6 shows the site–site pair distribution function $g(r)$ as a function of separation normalized by the radius of gyration. The solid (long dashed) curves show results for $S_0 = 0.3$ (10) for three values of N . At small r all curves approach $g(r=0) = 0$ continuously. Compared to the analogous simple globule model results (Figure 3) the interpenetrating ring liquids display a much sharper increase in $g(r)$ (weaker correlation hole) due to ring interpenetration. The inset of Fig. 6 shows the excess or non-random correlation function weighted by the surface area factor. At low dimensionless compressibility there are no oscillations, while for large compressibility weak oscillations and a small overshoot in $g(r)$ emerge. Compared to globules (Fig. 3 inset), the magnitude of $(r/R_g)^2 h(r)$ is much smaller. As found for globules (Fig. 4), ring polymers exhibit collective static structure factors $S(k)$ with no oscillatory behavior (not shown).

Figure 6 also shows an example of how the ring segment–segment pair correlations compare with a linear chain analog at fixed $N=1000$ and $S_0=10$. The chain result, computed using Eqs. (12)–(14), is shown by the short-dashed blue curves and should be compared to the long-dashed blue curve ring analog. Rings exhibit a correlation hole that extends to longer length scales, with stronger excess correlations.

These trends follow from dual nature of rings: globally space-filling in a qualitative sense but partially interpenetrating on smaller length scales due to their rough surfaces.

Figure 7 shows calculations of the mean number of nearest neighbor rings using Eq. (9) for $\tilde{R} = 1$ (solid) and 2 (dashed) as a function of N for S_0 varying from 0.5–15. For all cases, as ring size grows there is a dramatic increase in the number of neighboring rings until it tends to saturate at large enough N . This behavior is very different from both the behavior of the simple globule model where n_p is independent of N , and also that of linear chains where n_p grows in an unbounded manner as \sqrt{N} . The interpenetrating ring liquid displays behavior intermediate between linear chains and globules. Our results for the number of nearest neighbors mimic the effective volume fraction in the sense that $n_p \sim \phi_{eff}$. The inset of Fig. 7 investigates this in detail by plotting n_p/ϕ_{eff} as a function of N . Except at very low N (not relevant to polymer systems), the latter quantity is nearly constant with a proportionality constant that depends on \tilde{R} .

Finally, we compare our theoretical results for the number of nearest neighboring rings with three simulation studies [32–34]. Each simulation is different in detail with regards to the model adopted, the polymer concentration, and/or the precise manner (distance criterion) in which a nearest neighbor is defined. However, there are common features. Michiello and Turner (MT) [33] simulated a concentrated solution of rings with a relatively large local stiffness and a distance criterion of $2R_g$. It is their results for the intra-ring structure factor that we have employed in our theoretical analysis. Their system parameters are: $\rho_s \sigma_{LJ}^3 = 0.1$, $\sigma_k = 10 \sigma_{LJ}$, $C_\infty \approx 10$, and thus $\sigma = \sqrt{10} \sigma_{LJ}$. Since the polymer mean square end-to-end distance is $\langle R^2 \rangle = N \sigma_k \sigma_{LJ}$, the dimensionless segment level density in our model is estimated as $\rho_s \sigma^3 = \sqrt{10}$. From Eqs. (13) and (14)

this implies $S_0 \approx 1.1$. In a second study, Halverson, Lee, Grest, Grosberg, and Kremer (HLGGK) [34] employed the standard bead-spring Kremer–Grest (KG) model to study ring melts with systems parameters: $\rho_s \sigma_{LJ}^3 = 0.85$, $\sigma_k \sim C_\infty \sigma_{LJ}$, $C_\infty \approx 1.4$, and thus $\sigma = \sqrt{1.4} \sigma_{LJ}$. These parameters yield the estimate $\rho_s \sigma^3 \approx 1.4$. Then, using Eqs. (13) and (14) we estimate $S_0 \approx 6$. The third simulation study by Smerk and Grosberg (SM) [32] also employed a KG polymer model.

MT and HLGGK computed the number of nearest neighbor rings (n_p in our notation) based on a distance criterion ($r^* = R_g$), while SM computed a different geometric measure based on interpenetrating surfaces. MT found $n_p \sim 6-9$ as $N=256-2028$, following crudely a $N^{0.27}$ power law. HLGGK found that $n_p \sim 1.5-3$ for $N=10-2000$. However, if they choose the distance to define a neighbor to be the larger (by a factor of order 2) "ring end-to-end distance" they found $n_p \sim 11-16$, in reasonable accord with the findings of MT. SG found $n_p \sim 2-18$ for $N=10-1600$ based on their geometric criterion. So, although the models and criteria used in these simulation studies are not the same, all find n_p grows significantly with increasing ring size.

The n_p data from the three simulations discussed above are shown in Figure 8 along with our theoretical calculations for a range of S_0 values. As a quantitative caveat we note that the simulations of MT and HLGGK analyzed the number of nearest neighbors based on the $g(r)$ between rings at the center-of-mass level. This is not identical to our analysis based on the site–site $g(r)$ via Eq. (9), though the two are very close in spirit. Recall we employed the single ring structure factor of MT, for which we estimate $S_0 \sim 1.1$. Rather surprisingly, there is almost quantitative agreement between our $S_0=1$ calculations and the MT results. Even more surprising is that the HLGGK

simulations (for which we estimate $S_0 \sim 6$) almost quantitatively agree with our theoretical calculations for $S_0 = 5-10$ despite the fact that our $\omega(k)$ was constructed from the MT simulations. Qualitatively, the simulation results of SG also seem roughly consistent with our calculations, especially given the unavoidable uncertainties of determining the appropriate parameters of our coarse-grained thread model and the different geometric manner SG employed to define neighbors.

To summarize, liquids composed of ring polymers exhibit distinctly different behavior compared to their linear chain and simple globule model analogs. In a constant dimensionless compressibility ensemble, EOS effects lead to an increase in the effective ring volume fraction which have large consequences on packing structure. The effective volume fraction, which is proportional to the number of nearest neighboring rings, grows dramatically at intermediate N before nearly saturating at large N . This reflects the limited interpenetration of rings near their surface (Fig. 1b) and buttresses the physical picture of rings packing as an unusual realization of soft colloids.

V. DISCUSSION

We have developed a segment or site level statistical mechanical theory for the thermodynamics and real space pair structure of dense liquids of simple models of globules and interpenetrating ring polymers. The former is valuable as a baseline or reference system to compare with collapsed rings, and as a crude model of core-shell soft nano- or micron-sized particles with thin or non-existent coronas. To study ring polymer liquids, we constructed a two-fractal regime intra-ring structure factor model guided by simulation. At small length scales, it describes chain-like macromolecules, while globally the rings are collapsed. Motivated by recent simulations, theory and experiments, the

crossover between these two regimes was chosen to be mesoscopic, independent of ring size N , and of order the entanglement length of the chain analog.

For the simple globule model, we adopted a constant volume fraction ensemble relevant to suspension, and found that the equilibrium structure is independent of N . The dimensionless compressibility and pressure are predicted to vary exponentially with macromolecular volume fraction. Our analysis in Section II.C. suggests the simple globule model in conjunction with polymer integral equation theory provides a zeroth order understanding of the unusual equation-of-state behavior of dense suspensions of phytylglycogen nanoparticles [59]. The predicted inter-molecular correlations exhibit a correlation hole down to small length scales. The number of neighbors grows monotonically with volume fraction and does not saturate given the globules can overlap to some degree on the macromolecular scale even though they cannot at the segmental scale.

For the interpenetrating ring polymer liquids, we find dramatically different behavior. In this case, we adopted a constant compressibility ensemble motivated by simulation and experimental studies (and generic theoretical expectations), which find the ring and chain melt equations-of-state and density are very similar and not significantly N -dependent under isobaric conditions. The effective volume fraction grows at intermediate N since changing macromolecular size modulates the relative importance of the limited interpenetration in ring liquids. However, the latter appears to be essentially bound for very large rings, displaying a near plateau behavior with a slow logarithmic increase. The intermolecular segment–segment correlations are weaker than for the simple globule model in the sense that the correlation hole is shallower, however the

suppression of $g(r)$ below the random value remains stronger than for linear chains. More importantly, the number of neighboring rings increases dramatically at small N , akin to linear polymer chains, but tends to saturate at large N . Our results agree rather well with different simulation studies for the absolute values of the number of neighboring rings in concentrated solution and melts and how they vary with N . More generally, we expect the theoretical approach and tools developed here are relevant for other complex fluids composed of soft partially interpenetrating objects such as core-shell microgels and nanogels, hairy colloids, and highly-branched dendritic nanoparticles.

Going forward, we will use the present structural theory to develop a predictive approach at the segmental scale for the dynamics of liquids composed of globular objects and ring polymers. The dramatic increase of effective volume fraction and number of neighboring molecules for rings raises the possibility of a "topological" glass-like transition induced by increasing N , as recently suggested in simulation studies [33,38]. The advance reported here in conjunction with our new generalized Rouse model [53] provides a foundation to understand such a glass-like transition and the ring center-of-mass dynamics and diffusion constant.

Acknowledgments The authors thank Dimitris Vlassopoulos, Hiroshi Watanabe, Charles Schroeder, and John Dutcher for informative exchanges. This work was performed at the University of Illinois and supported by DOE-BES under Grant No. DE-FG02-07ER46471 administered through the Frederick Seitz Materials Research Laboratory.

References

- [1] A. Carlmark, C. Hawker, A. Hult and M. Malkoch, *Chemical Society Reviews*, 2009, **38**, 352.
- [2] M. Rubinstein and R. H. Colby, *Polymer Physics*, Oxford University Press, Oxford, UK, 2003.
- [3] P. G. deGennes, *Scaling Concepts in Polymer Physics*, Cornell University Press, Ithaca, NY, USA, 1979.
- [4] R. G. Larson and P. S. Desai, *Annual Review of Fluid Mechanics*, 2015, **47**, 47.
- [5] D. Vlassopoulos, *Rheologica Acta*, 2016, **55**, 613.
- [6] C. M. Roland, *Rubber Chemistry and Technology*, 2012, **85**, 313.
- [7] A. E. Likhtman, *Soft Matter*, 2014, **10**, 1895.
- [8] J. D. Halverson, J. Smrek, K. Kremer, and A. Y. Grosberg, *Reports on Progress in Physics*, 2014, **77**, 022601.
- [9] M.Imakev, K.Tchovrina, S.Nechaev and L.Mirny, *Soft Matter*, 2015, **11**, 665.
- [10] A.Certovich and P.Kos, *Journal of Chemical Physics*, 2014, **141**, 13393.
- [11] S.Obukhov, A.Johner, J.Baschnagel, H.Meyer and J.P.Wittmer, *Europhysics Letters*, 2014, **105**, 48005.
- [12] A. Grosberg, *Soft Matter*, 2014, **10**, 560.
- [13] M. Kapnistos, M. Lang, D. Vlassopoulos, W. Pyckhout-Hintzen, D. Richter, D. Cho, T. Chang and M. Rubinstein, *Nature Materials*, 2008, **7**, 997.
- [14] R. Pasquino, T. C. Vasilakopoulos, Y. C. Jeong, H. Lee, S. Rogers, G. Sakellariou, J. Allgaier, A. Takano, A. R. Bras, T. Chang, S. Goosen, W. Pyckhout-Hintz, A.

Wischnewski, N. Hadjichristidis, D. Richter, M. Rubinstein and D. Vlassopoulos, *ACS MacroLetters*, 2013, **2**, 874.

[15] Y. Doi, A. Matsumoto, T. Inoue, T. Iwamoto, A. Takano, Y. Matsushita, Y. Takahashi and H. Watanabe, *Rheologica Acta*, 2017, **56**, 567.

[16] D. Richter, S. Goosen and A. Wischnewski, *Soft Matter*, 2015, **11**, 8535.

[17] A. R. Bras, S. Goosen, M. Krutyeva, A. Radulescu, B. Farago, J. Allgaier, W. Pyckhout-Hintzen, A. Wischnewski and D. Richter, *Soft Matter*, 2014, **10**, 3649.

[18] P. Bačová, F. Lo Verso, A. Arbe, J. Colmenero, J. A. Pomposo, and A. J. Moreno, *Macromolecules*, 2017, **50**, 1719.

[19] A. Arbe, J. Pomposo, A. Moreno, F. LoVerso, M. González-Burgos, I. Asenjo-Sanz, A. Iturrospe, A. Radulescu, O. Ivanova, and J. Colmenero, *Polymer*, 2016, **105**, 532.

[20] M. González-Burgos, A. Arbe, A. J. Moreno, J. A. Pomposo, A. Radulescu, and J. Colmenero, *Macromolecules*, 2018, **51**, 1573.

[21] J. De-La-Cuesta, E. González, and J. A. Pomposo, *Molecules*, 2017, **22**, 1819.

[22] J. Rubio-Cervilla, E. González, and J. A. Pomposo, *Nanomaterials*, 2017, **7**, 341.

[23] E. R. Gillies and J. M. Frechet, *Drug Discovery Today*, 2005, **10**, 35.

[24] N. C. Seeman and H. F. Sleiman, *Nature Reviews Materials*, 2017, **3**, 17068.

[25] K. J. De France, T. Hoare, and E. D. Cranston, *Chemistry of Materials*, 2017, **29**, 4609.

[26] M. Bohn and D. W. Heermann, *Journal of Chemical Physics*, 2010, **132**, 044904.

[27] Z.-J. Tan and S.-J. Chen, *Biophysical Journal*, 2012, **103**, 827.

- [28] G. J. Smith, K. T. Lee, X. Qu, Z. Xie, J. Pesic, T. R. Sosnick, T. Pan and N. F. Scherer, *Journal of Molecular Biology*, 2008, **378**, 943.
- [29] H. Zhang, C. Schwartz, G. M. De Donatis and P. Guo, *Advances in Virus Research*, 2012, **83**, 415.
- [30] F. Ding, C. Lu, W. Zhao, K. R. Rajashankar, D. L. Anderson, P. J. Jardine, S. Grimes and A. Ke, *Proceedings of the National Academy of Sciences*, 2011, **108**, 7357.
- [31] S. Brown and G. Szamel, *Journal of Chemical Physics*, 1998, **108**, 4705.
- [32] J. Smrek and A. Y. Grosberg, *ACS Macro Letters*, 2016, **5**, 750.
- [33] D. Michieletto and M. S. Turner, *Proceedings of the National Academy of Sciences*, 2016, **113**, 5195.
- [34] J. D. Halverson, W. B. Lee, G. S. Grest, A. Y. Grosberg and K. Kremer, *Journal of Chemical Physics*, 2011, **134**, 204904.
- [35] J. D. Halverson, W. B. Lee, G. S. Grest, A. Y. Grosberg and K. Kremer, *Journal of Chemical Physics*, 2011, **134**, 204905.
- [36] J. D. Halverson, G. S. Grest, A. Y. Grosberg and K. Kremer, *Physical Review Letters*, 2012, **108**, 038301.
- [37] W.-C. Lo and M. S. Turner, *Europhysics Letters*, 2013, **102**, 58005.
- [38] D. Michieletto, N. Nahali and A. Rosa, *Physical Review Letters*, 2017, **119**, 197801.
- [39] E. Lee, S. Kim and Y. Jung, *Macromolecular Rapid Communications*, 2015, **36**, 1115.
- [40] A. Rosa and R. Everaers, *Physical Review Letters*, 2014, **112**, 118302.
- [41] J. P. Wittmer, H. Meyer, A. Johner, S. Obukhov and J. Baschnagel, *Journal of Chemical Physics*, 2013, **139**, 217101.

- [42] A.Rosa and R.Everaers, *PLoS Computational Biology* 2008, **4**, e1000153.
- [43] A.Rosa, N.B.Becker and R.Everaers, *Biophysical Journal* 2010, **98**, 2410.
- [44] R. Pasquino, T. C. Vasilakopoulos, Y. C. Jeong, H. Lee, S. Rogers, G. Sakellariou, J. Allgaier, A. Takano, A. R. Brás, T. Chang, S. Gooßen, W. Pyckhout-Hintzen, A. Wischnewski, N. Hadjichristidis, D. Richter, M. Rubinstein and D. Vlassopoulos, *ACS Macro Letters*, 2013, **2**, 874.
- [45] D. G. Tsalikis, T. Koukoulas, V. G. Mavrantzas, R. Pasquino, D. Vlassopoulos, W. Pyckhout-Hintzen, A. Wischnewski, M. Monkenbusch, and D. Richter, *Macromolecules*, 2017, **50**, 2565.
- [46] S. Gooßen, A. R. Brás, W. Pyckhout-Hintzen, A. Wischnewski, D. Richter, M. Rubinstein, J. Roovers, P. J. Lutz, Y. Jeong, T. Chang, and others, *Macromolecules*, 2015, **48**, 1598.
- [47] T. Ge, S. Panyukov and M. Rubinstein, *Macromolecules*, 2016, **49**, 708.
- [48] L. J. Fetters, D. J. Lohse, D. Richter, T. A. Witten, and A. Zirkel, *Macromolecules*, 1994, **27**, 4639.
- [49] K. S. Schweizer and J. G. Curro, *Advances in Chemical Physics*, 1997, **98**, 1.
- [50] M. Fuchs, *Zeitschrift für Physik B: Condensed Matter*, 1997, **103**, 521.
- [51] V. Krakoviack, J. Hansen and A. Louis, *Europhysics Letters*, 2002, **58**, 53.
- [52] G. Yatsenko, E. Sambriski, M. Nemirovskaya, and M. Guenza, *Physical Review Letters*, 2004, **93**, 257803.
- [53] Z. E. Dell and K. S. Schweizer, *Journal of Chemical Physics*, 2017, **146**, 134901.
- [54] K. S. Schweizer, *Journal of Chemical Physics*, 1989, **91**, 5802.

- [55] J. P. Hansen and I. R. McDonald, *Theory of Simple Liquids*, Academic, London, UK, 1986.
- [56] M. Fuchs and K. S. Schweizer, *Journal of Chemical Physics*, 1997, **106**, 347.
- [57] M. Cates, *Physical Review Letters*, 1984, **53**, 926.
- [58] M. Muthukumar, *Journal of Chemical Physics*, 1985, **83**, 3161.
- [59] H. Shamana, M. Grossutti, E. Papp-Szabo, C. Miki and J. R. Dutcher, *Soft Matter*, 2018, **14**, 6496.
- [60] R. Everaers, *Physical Review E*, 2012, **86**, 022801.
- [61] R. T. Bonnecaze and M. Cloitre, *Advances in Polymer Science*, 2010, **236**, 117.
- [62] D. Banerjee and K. S. Schweizer, *Journal of Chemical Physics*, 2015, **142**, 214903.

Figures

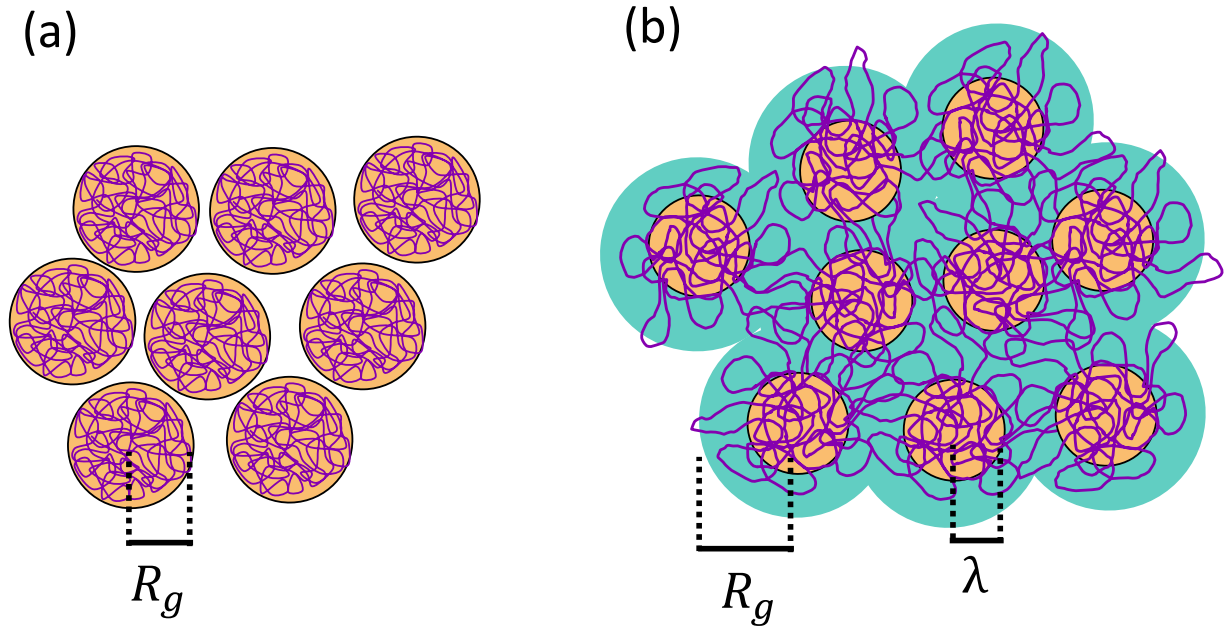


Figure 1 - Schematic cartoons of the studied models. (a) In the simple globule model the qualitative picture is that polymers (purple curves) are collapsed into compact structures (orange spheres) characterized by a radius of gyration, $R_g \sim N^{1/3}$. (b) Per simulation studies, rings behave in a compact manner at large scales but a chain-like manner on smaller internal scales that allow them to interpenetrate in a limited manner (teal spherical shells). The crossover length scale from space filling to interpenetrating behavior is λ and is taken to be independent of the ring degree of polymerization N .

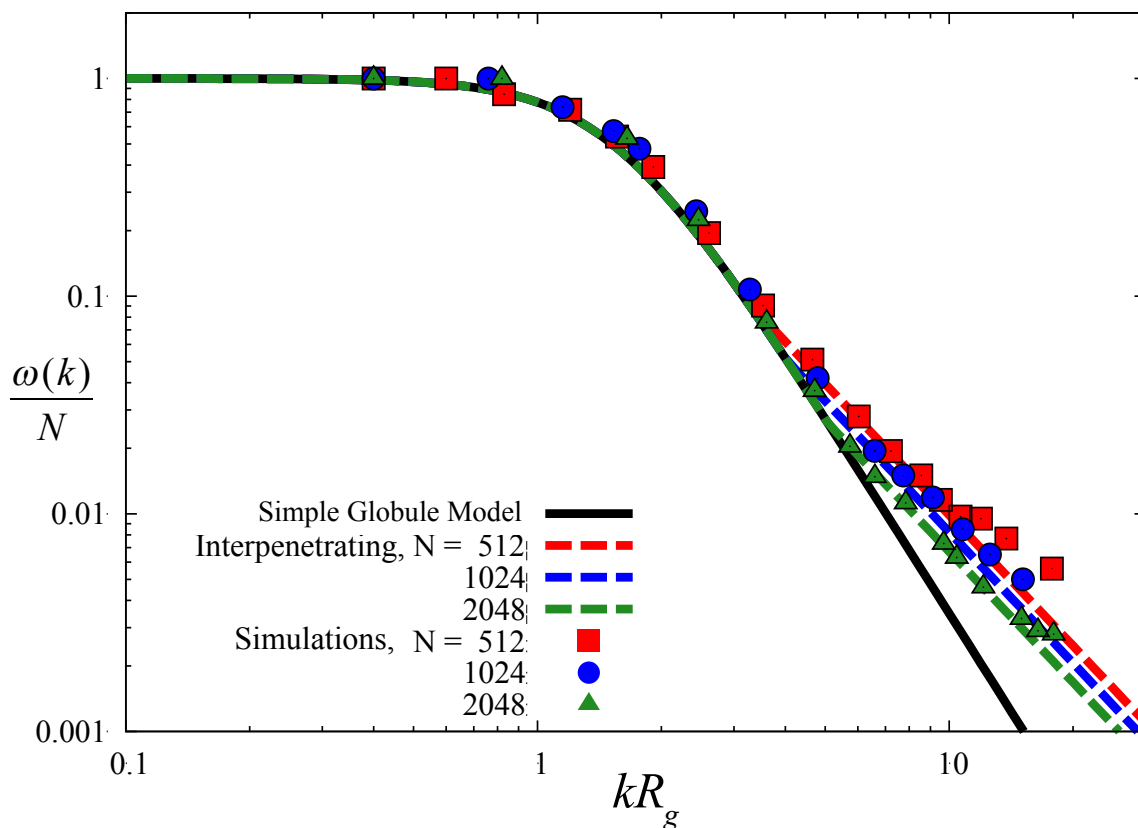


Figure 2 - The intra-molecular structure factor normalized by the degree of polymerization, $\omega(k)/N$, as a function of wavevector normalized by ring radius of gyration, kR_g . The points show simulation data [33] for three different ring sizes. The solid black curve is the adopted simple globule model of Eq. (15) with $A = 0.286$. The dashed curves are the ring polymer model of Eq. (20).

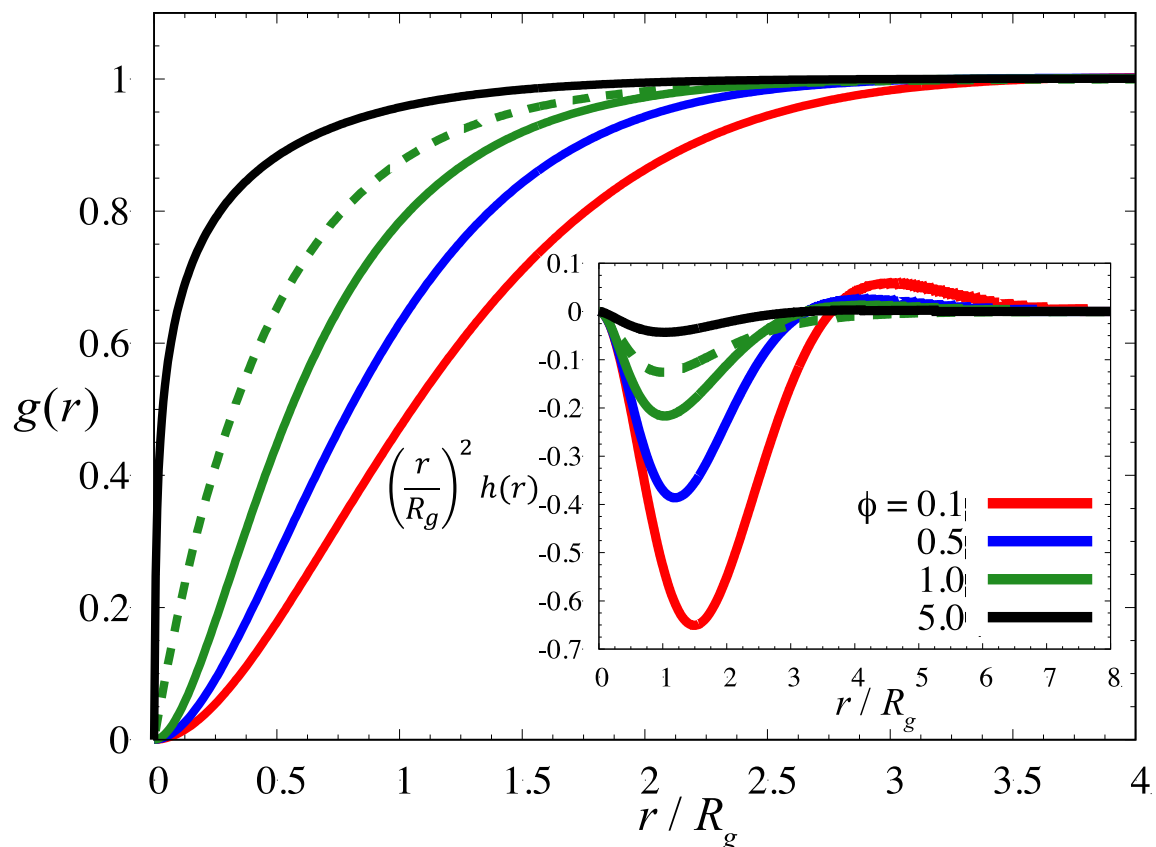


Figure 3 – Intermolecular site–site pair correlation function, $g(r)$, for the simple globule model fluid as a function of inter-site separation in units of the radius of gyration, r/R_g , for macromolecular volume fractions $\phi = 0.1, 0.5, 1.0,$ and 5.0 (solid curves from right to left). (inset) The surface area weighted excess correlations $(r/R_g)^2 h(r)$ as a function of separation for the same systems (lowest ϕ system is bottom solid curve at $r = 1.5 R_g$). In both the main frame and inset the dashed curves are the analogous chain liquid result for

$$\phi = 1.0.$$

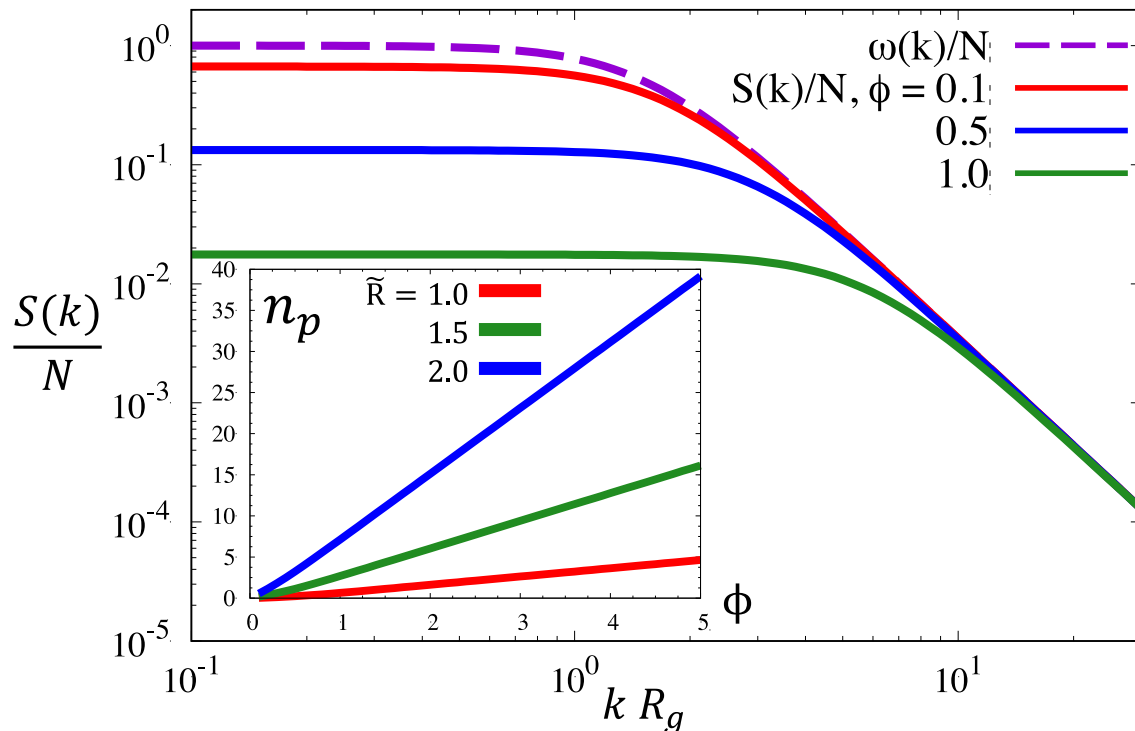


Figure 4 – (main) Collective segment-level density fluctuation structure factor of the simple globule model liquid normalized by the degree of polymerization N (solid curves) as a function of the dimensionless wave vector for three macromolecular volume fractions $\phi = 0.1, 0.5,$ and 1.0 (solid curves from top to bottom at low k). The intra-molecular structure factor $\omega(k)$ (dashed curve) is shown for reference. (inset) The number of nearest neighbor globules surrounding a tagged globule as a function of ϕ for 3 choices of nearest neighbor criterion $\tilde{R} = r^*/R_g = 1, 1.5, 2$ (bottom to top).

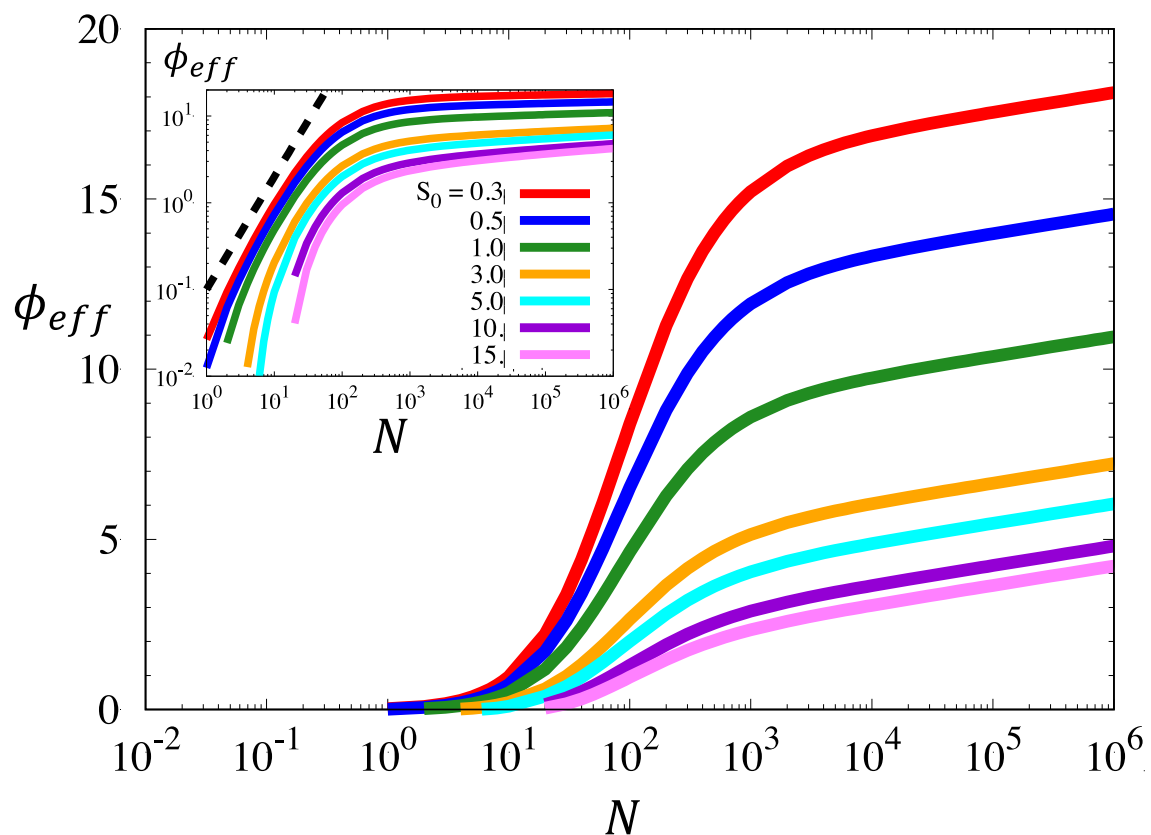


Figure 5 – Effective macromolecular volume fraction for the interpenetrating ring polymer liquid as a function of N . The fixed dimensionless compressibilities range from $S_0 = 0.3$ to 15 (top to bottom). The main (inset) plot is in a linear–log (log–log) representation. The black dashed line in the inset shows the power law $N^{1.3}$ for reference.

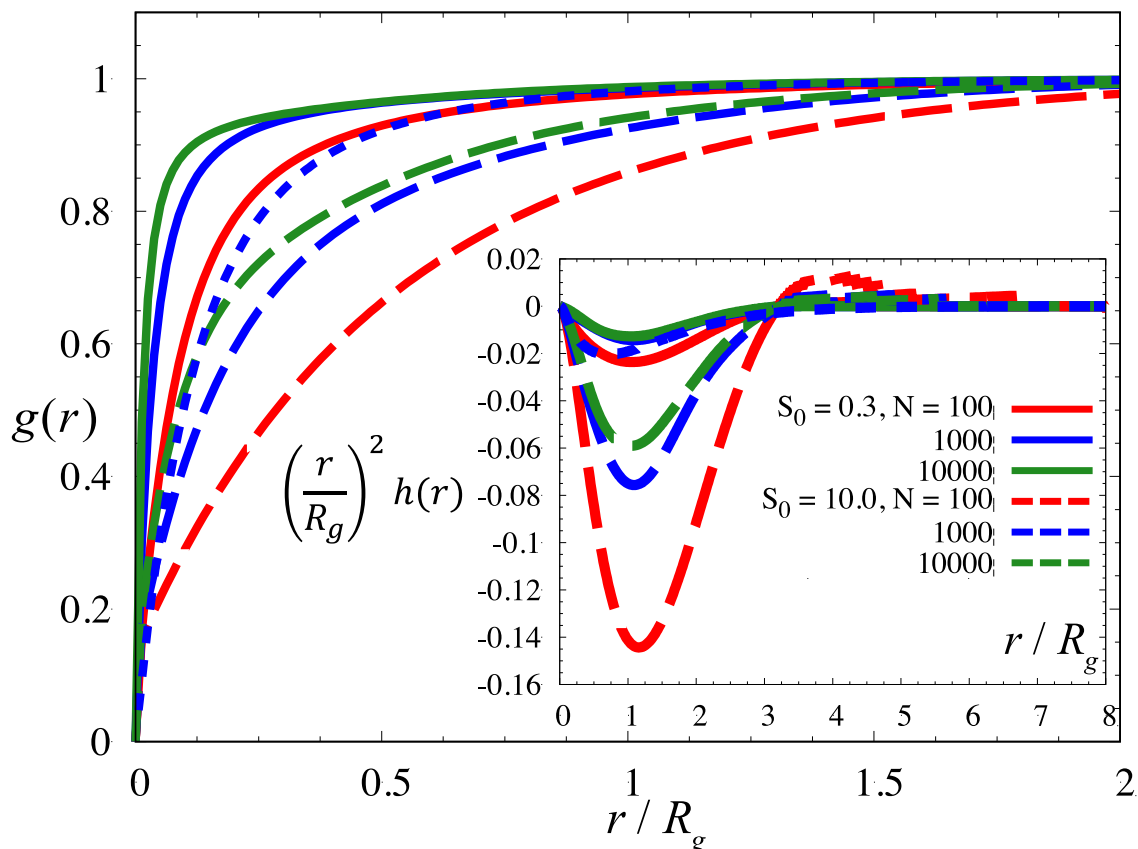


Figure 6 – Site–site intermolecular pair correlation function for ring polymer liquids as a function of separation relative to the radius of gyration for two dimensionless compressibilities $S_0 = 0.3$ (solid) and 10.0 (dashed). For each S_0 , results for three N values are shown. For $S_0 = 0.3$ (10.0) the effective volume fractions are $\phi_{eff} = 8.4, 15.2,$ and 17.1 (1.3, 2.9, and 3.6) for $N = 100, 1000,$ and 10000 , respectively. (inset) The excess correlation function multiplied by the surface area factor as a function of separation for the same systems as the main frame. In both the inset and the main frame, the short-dashed blue curve shows the chain liquid analog for $S_0 = 10.0$ and $N = 1000$.

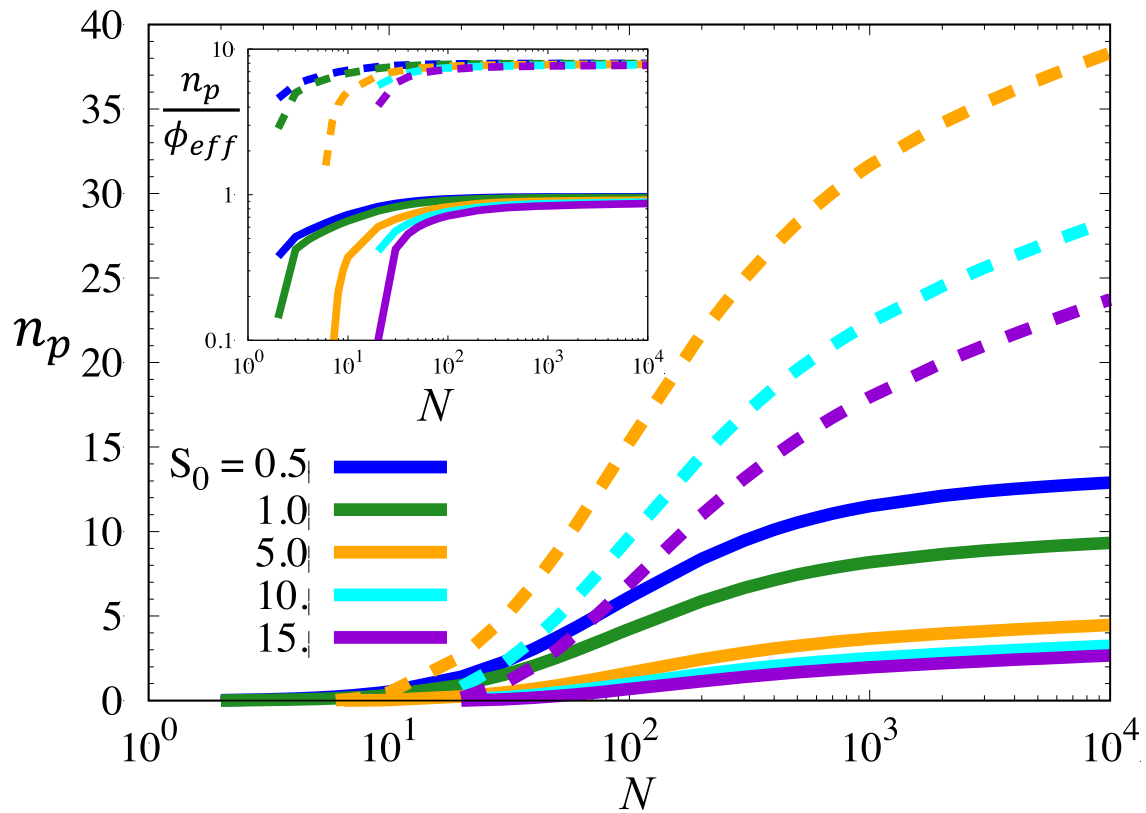


Figure 7 – Number of nearest neighbor rings as a function of N . The solid curves employ the distance criterion $\tilde{R} = 1$, and $S_0 = 0.5, 1.0, 5.0, 10,$ and 15 (from top to bottom). The dashed curves employ $\tilde{R} = 2$, with $S_0 = 5.0, 10,$ and 15 (from top to bottom). (inset) Same as main frame where n_p is divided by the effective volume fraction ϕ_{eff} .

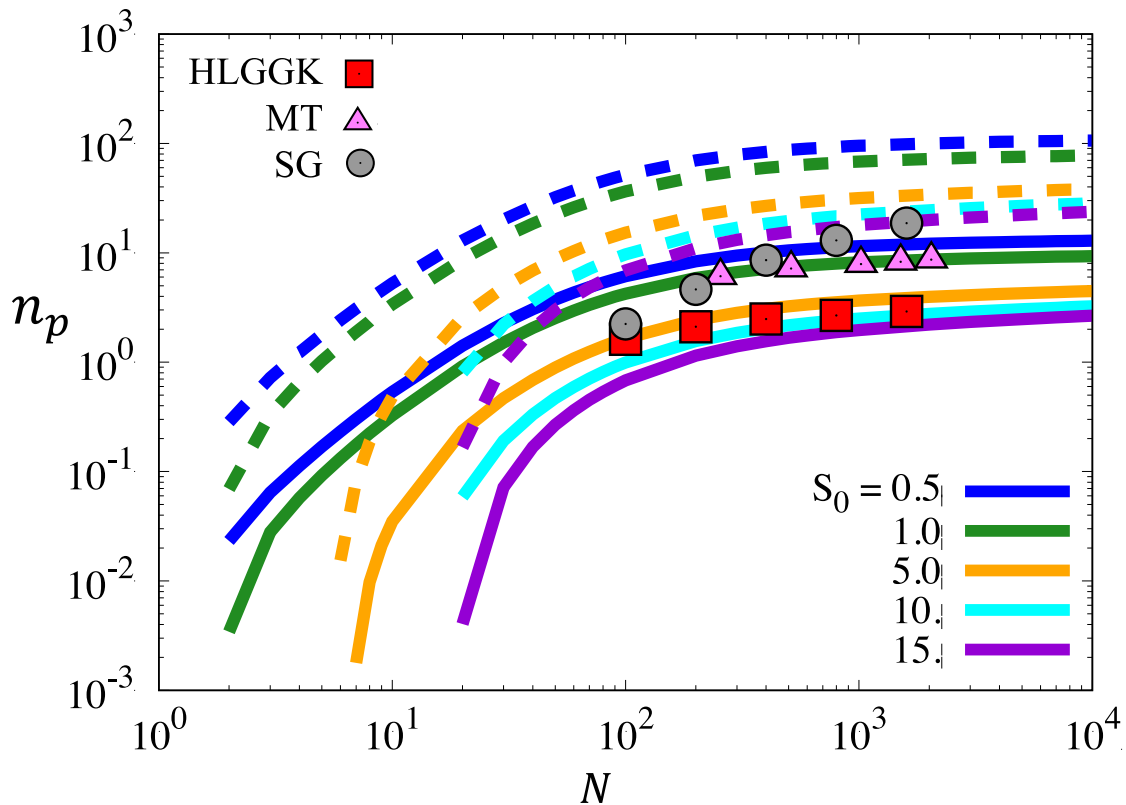


Figure 8 – Comparison of simulation results with our theoretical calculations for the number of nearest neighbor rings. The latter are the same as the main frame of Figure 7 but in a log–log representation. Results from three simulations are shown as points: squares from Halverson, Lee, Grest, Grosberg, and Kremer (HLGGK, Ref. [34]); triangles from Michieletto and Turner (MT, Ref. [33]); and circles from Smrek and Grosberg (SG, Ref. [32]).

Table of Contents

Intermolecular segment–segment pair distribution function $g(r)$

